

N ab : M easurem ent P rinciples, A pparatus and U ncertainties

D inko P ocanic^{a,i}, R . A larcon^b, L . P . A lonzi^a, S . Bae ler^a,
S . B alascuta^b, J . D . B owm an^h, M . A . B ychkov^a, J . B yme^j,
J . R . C alarco^f, V . C ianciolo^h, C . C raw ford^c, E . F rlez^a,
M . T . G ericke^d, G . L . G reene^k, R . K . G rzyw acz^k, V . G udkovⁱ,
F . W . H ersm an^f, A . K lein^e, J . M artin^g, S . A . Page^d,
A . P alladino^a, S . I . P enttila^h, K . P . R ykaczew ski^h,
W . S . W ilbum^e, A . R . Young^g, G . R . Young^h

The N ab collaboration

^aD epartm ent of P hysics, U niversity of V irginia, C harlottesville, VA 22904, U SA

^bD epartm ent of P hysics, A rizona State U niversity, Tem pe, A Z 85287-1504, U SA

^cD epartm ent of P hysics and A stron om y, U niversity of K entucky, Lexington,
K entucky 40506, U SA

^dD epartm ent of P hysics and A stron om y, U niversity of M anitoba, W innipeg,
M anitoba, R 3T 2N 2 C anada

^eLos A lam os N ational Laboratory, Los A lam os, NM 87545, U SA

^fD epartm ent of P hysics, U niversity of New H am pshire, D urham , NH 03824, U SA

^gD epartm ent of P hysics, N orth C arolina State U niversity, R aleigh, NC
27695-8202, U SA

^hP hysics D ivision, O ak R idge N ational Laboratory, O ak R idge, TN 37831, U SA

ⁱD epartm ent of P hysics and A stron om y, U niversity of South C arolina, C olum bia,
SC 29208, U SA

^jD epartm ent of P hysics and A stron om y, U niversity of Sussex, B righton, BN19RH,
U K

^kD epartm ent of P hysics and A stron om y, U niversity of Tennessee, K noxville, TN
37996-1200, U SA

^lD epartm ent of P hysics, U niversity of W innipeg, W innipeg, M anitoba, R 3B 2E9
C anada

Abstract

The Nab collaboration will perform a precise measurement of a , the electron-neutrino correlation parameter, and b , the Fierz interference term in neutron beta decay, in the Fundamental Neutron Physics Beam line at the SNS, using a novel electric/magnetic field spectrometer and detector design. The experiment is aiming at the 10^{-3} accuracy level in a , and will provide an independent measurement of $\lambda = G_A/G_V$, the ratio of axial-vector to vector coupling constants of the nucleon. Nab also plans to perform the first ever measurement of b in neutron decay, which will provide an independent limit on the tensor weak coupling.

Key words: neutron beta decay, correlations, precision measurement

PACS: 13.30.Ce, 14.20.Dh, 23.40.-s, 24.80.-y

1 Motivation

Neutron beta decay provides one of the most sensitive means for exploring details and limits of our understanding of the weak interaction. Thanks to its highly precise theoretical description [1], neutron decay is sensitive to contributions from processes not included in the standard model (SM) of particles and interactions (for comprehensive reviews see Refs. [2,3,4]). Neglecting recoil, radiative and loop corrections, the differential decay rate for unpolarized neutrons is given by parameters a and b : $dw/d\Omega_e = 1 + a \cos \theta_e + b(m_e/E_e)$, where $\theta_e = \mathbf{p}_e \cdot \mathbf{E}_e$, p_e , E_e and θ_e are the electron momentum, energy, and opening angle, respectively [5]. The $\cos \theta_e$ correlation parameter a , and the asymmetry parameters with respect to the neutron spin: A (beta), B (neutrino), and C (proton; $C \propto A + B$ in leading order) possess complementary dependencies on the ratio of Fermi constants $\lambda = G_A/G_V$, as well as on operators that depart from the $(\bar{V} A) (V A)$ form of the SM charged current (CC) weak interaction. Additionally, b , the Fierz interference term, offers an independent test of scalar and tensor admixtures arising in broad classes of L-R mixing SUSY extensions. Thus precise measurements of neutron decay parameters offer the distinct advantage of overconstrained independent checks of the SM predictions, as well as the potential for indicating or ruling out certain types of extensions to the SM $(\bar{V} A) (V A)$ form [2,3,4,6]. Hence, a set of appropriately precise measurements of the neutron decay parameters a , b , A , and B will have considerably greater physics implications than the erstwhile predominant experimental focus on A , i.e., λ . At a minimum,

Corresponding author: pocanic@virginia.edu

such a data set combined with new measurements of the neutron lifetime, τ_n , will enable a definitive resolution of the persistent discrepancies in a and Cabibbo-Kobayashi-Maskawa (CKM) matrix element V_{ud} [7].

The Nab collaboration [8] has undertaken to carry out precise measurements of a , the e - $\bar{\nu}_e$ correlation parameter, and b , the so far unmeasured Fierz interference term, in neutron decay. Goal accuracies are $\delta a = a \times 10^{-3}$ and $\delta b = b \times 10^{-3}$. A novel 4 π solid-expansion spectrometer based on ideas outlined in Ref. [11] will be used in the Fundamental Neutron Physics Beam line (FnPB) at the Spallation Neutron Source (SNS) at Oak Ridge, Tennessee.

The Nab experiment constitutes the first phase of a program of measurements that will continue with second-generation measurements of spin correlations in neutron decay. The next experiment, named 'abBA', will measure parameters A and B in addition to a and b . In addition, the proton asymmetry C will be measured with the same apparatus. Together, Nab and abBA form a complete program of measurements of the main neutron decay parameters in a single apparatus with shared systematics and consistency checks. The experiments are complementary: Nab is highly optimized for the measurement of a and b , while abBA focuses on A and B with a lower-precision consistency check of the a and b parameters. Nab joins two existing experiments, aSPECT [9] and aCORN [10], which also study a .

2 Measurement Principles and Apparatus

The correlation parameter of interest, a , measures the dependence of the neutron beta decay rate on the cosine of the e - $\bar{\nu}_e$ relative angle. The Nab method of determination of a relies on the linear dependence of $\cos \theta_e$ on p_p^2 , the square of the proton momentum for a given electron momentum (or energy). Conservation of momentum gives the relation

$$p_p^2 = p_e^2 + 2p_e p \cos \theta_e + p^2; \quad (1)$$

where, to a very good approximation, p depends only on E_e (or p_e). Thus, Eq. 1 reduces to a linear relation between $\cos \theta_e$ and p_p^2 for a fixed p_e . The mapping of $\cos \theta_e$ and p_p^2 is shown graphically in Fig. 1. In this plot, the phase space alone distributes proton events evenly in p_p^2 between the lower and upper bounds for any fixed value of E_e . Given the linear relationship between p_p^2 and $\cos \theta_e$, the slope of the p_p^2 probability distribution is determined by the correlation parameter a ; in fact it is given by a , where $\beta = v_e/c$ (see Fig. 2). This observation leads to the main principle of measurement of a which involves measurement of the proton momenta via the proton time of flight (TOF), t_p , in a suitably constructed magnetic spectrometer. Ideally, the

magnetic field longitudinalizes the proton momentum and $t_p / 1 = t_p$; t_p is measured as the difference between the arrival times of the electron and the proton at the detector(s). In the present discussion we neglect the electron TOF. Parameter a is determined from the slopes of the $1 = t_p^2$ distributions for different values of E_e . If a were null, all distributions would have a slope of zero. Having multiple independent measurements of a for different electron energies provides a powerful check of systematics, as discussed below. The Fierz interference term b is determined from the shape of the measured electron energy spectrum.

For fixed E_e , a perfect spectrometer would record a trapezoidal distribution of $1 = t_p^2$ with sharp edges. The precise location of these edges is determined by well-defined kinematic cuts that only depend on E_e . However, a realistic time-of-flight spectrometer will produce imperfect measurements of the proton momenta due to the spectrometer response function, discussed in Sect. 3. The measured locations and shapes of edges in $1 = t_p^2$ distributions will allow us to examine the spectrometer response function and verify that the fields have been measured correctly.

The main requirements on the spectrometer are:

- (1) The spectrometer and its magnetic (B) and electric (E) fields are de-

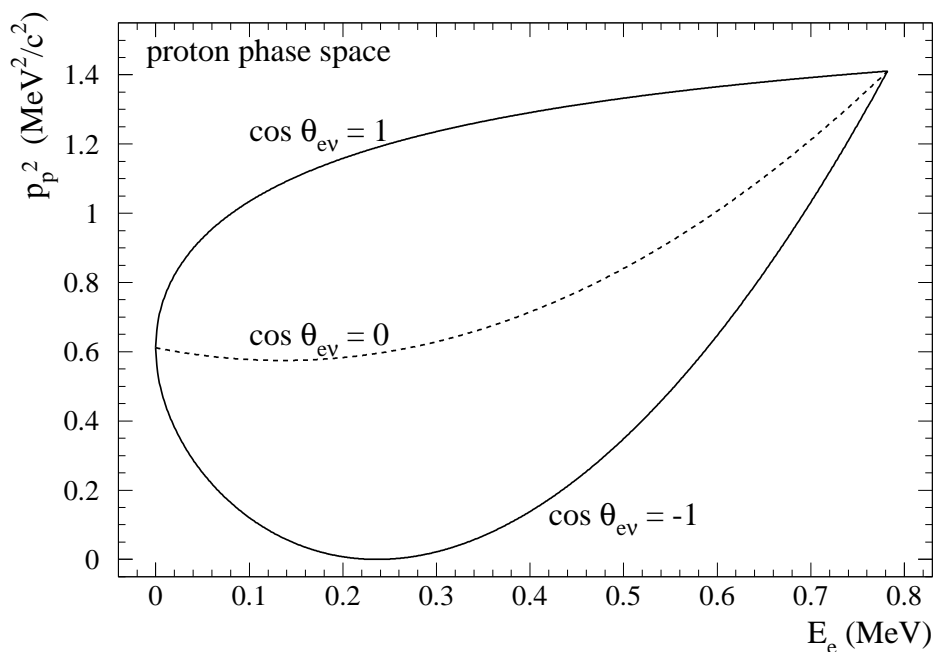


Fig. 1. Proton phase space (in terms of p_p^2) in neutron beta decay as a function of electron kinetic energy. The upper bound of the allowed phase space occurs for collinear e and p momenta, $\cos \theta_{ev} = 1$, while the momenta are anticollinear, $\cos \theta_{ev} = -1$, at the lower bound. The central dashed parabola corresponds to orthogonal e and p momenta.

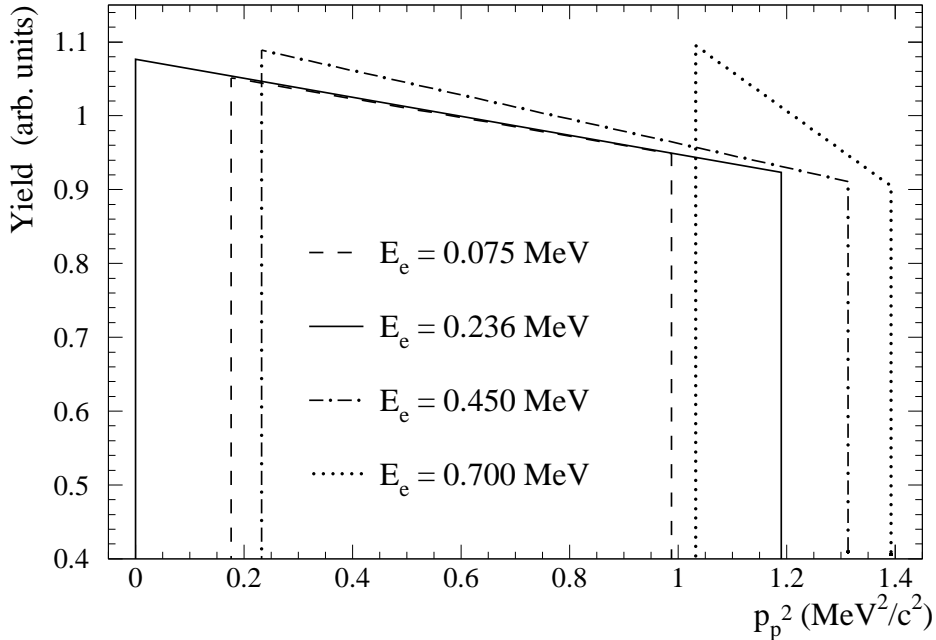


Fig. 2. A plot of proton yield for four different electron kinetic energies with $a = 0.105$. If a were 0, all the distributions would have a slope of 0. Vertical scale origin is suppressed.

signed to be azimuthally symmetric about the central axis, z .

- (2) Neutrons must decay in a region of large B' . The resulting protons and electrons spiral around a magnetic field line.
- (3) An electric field is required to accelerate the proton from the eV-range energies to a detectable energy range prior to reaching the detector. This field imposes, however, an energy threshold on e detection.
- (4) The proton momentum must rapidly become parallel to the magnetic field direction to ensure that the proton time of flight $t / l = p_p$. This requirement dictates a sharp field curvature (d^2B_z/dz^2) at the origin, followed by a sharp falloff of B_z .

The basic concept of the spectrometer consists of collinear solenoids with their longitudinal axis oriented normal to the neutron beam, which passes through the solenoid center. The solenoidal magnetic field starts out high at the position of the neutron beam, typically 4 T, dropping off quickly to parallelize the momenta as protons enter the long "drift" region. In the detection region at either end of the solenoid the field is increased to 1/4 of its central peak value. Cylindrical electrodes (consisting of three sections) maintain the neutron decay region at a potential of +30 kV with respect to the ends of the solenoid where detectors are placed at ground potential.

The magnetic field strength is sufficiently high to constrain both electrons and protons from neutron decay to spiral along the magnetic field lines with the component of the spiral motion transverse to the field limited by cyclotron

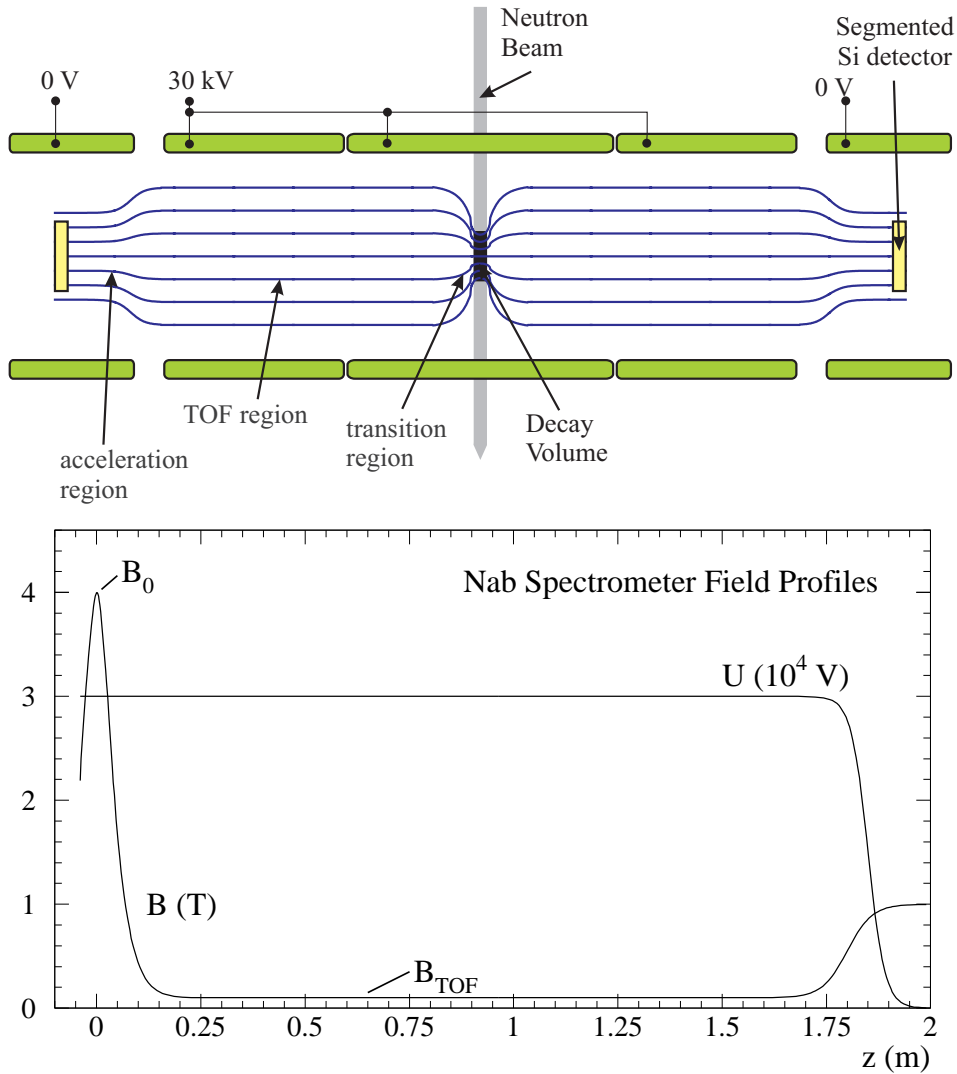


Fig. 3. Top panel: A schematic view of the vertical field expansion spectrometer showing the main regions of the device: (a) neutron decay region, (b) transition region with expanding magnetic field, (c) drift (TOF) region, and (d) the acceleration region before the detector. Bottom panel: Electrical potential (U) and magnetic field (B) profiles on axis for 1/2 of the Nab spectrometer length.

radii of the order of a few millimeters.

Hence, two segmented Si detectors, one at each end of the solenoid, view both electrons and protons in an effective 4 geometry. The time of flight between the electron and proton is accurately measured in a long, 1.5 meter, drift distance. The electron energy is accurately measured in the Si detectors. The proton momentum and electron energy determine the electron-neutrino opening angle. We note that by sorting the data on proton time of flight and electron energy, θ can be determined with a statistical uncertainty that is only 4% greater than the theoretical minimum [14].

A not-to-scale schematic view of the field expansion spectrometer is shown in Fig. 3. Electrons and protons spiral around magnetic field lines and are guided to two segmented Si detectors, each having a 100 cm^2 active area, and depicted schematically in Fig. 4. In the center of the spectrometer the axial field strength is 4 T , in the drift region 0.1 T , and near the Si detectors 1 T (see Fig. 3).

In a realistic spectrometer, however, the perfect one-to-one correspondence of proton momentum and time of flight is lost, due to imperfect momentum longitudinalization and other systematic effects, such as the lateral size of the neutron beam in the decay region. In other words, the detector response function instead of being a delta function in $1=t_p^2$ for each value of p_p^2 , becomes a broadened function, such as the ones calculated for three proton momenta and depicted in Fig. 5. The key challenge of the Nab approach to measuring a_1 is to minimize the width of the detector response function while keeping the relevant systematics under control. The resulting TOF distributions no longer have sharply cut-off edges as in Fig. 2. A sample set of results of GEANT 4 [12] Monte Carlo calculations for three electron energies is shown in Fig. 6.

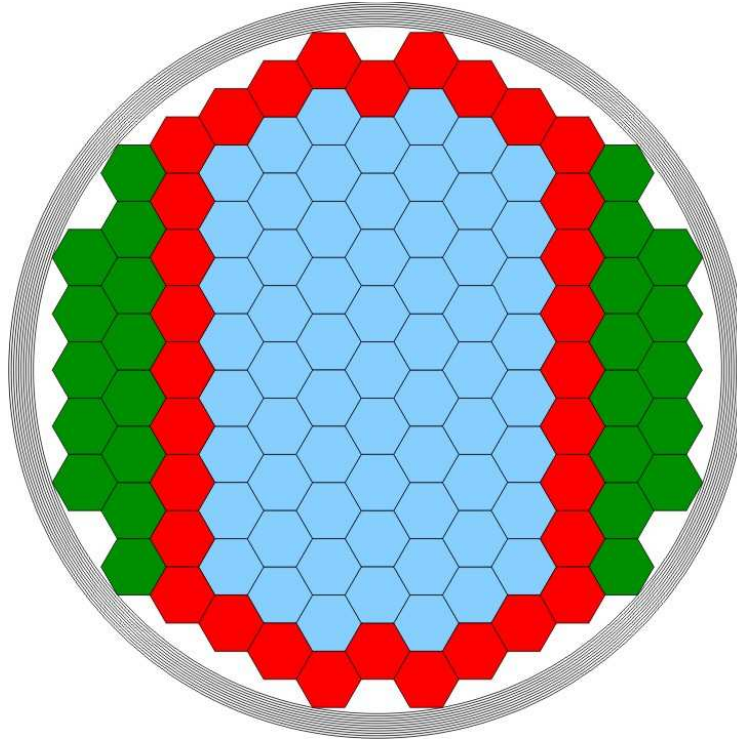


Fig. 4. Design for the ohmic side of the detector. The 127 hexagons represent individual detector elements. Proton events in the interior hexagons generate a valid trigger, while the perimeter hexagons are used only for detecting electrons. The concentric circles represent the guard ring structure. Electrical contact is made to each hexagon to provide the bias voltage and collect the charge deposited by incident particles. The areas between the pixels and guard rings are electrically connected to form one additional channel.

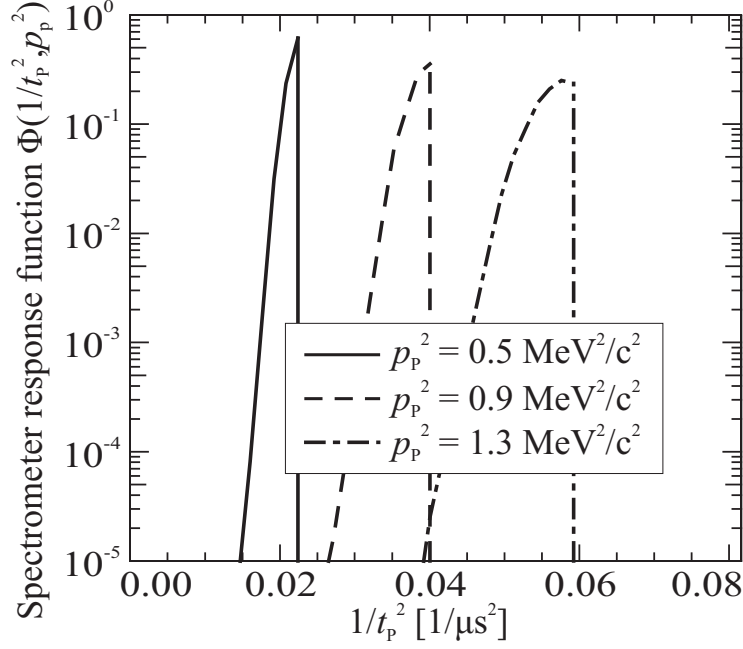


Fig. 5. Nab spectrometer response function, shown for different proton momenta, the magnetic field from Fig. 3 and a centered neutron beam with a width of 2 cm. The calculation assumes full adiabaticity of the proton motion.

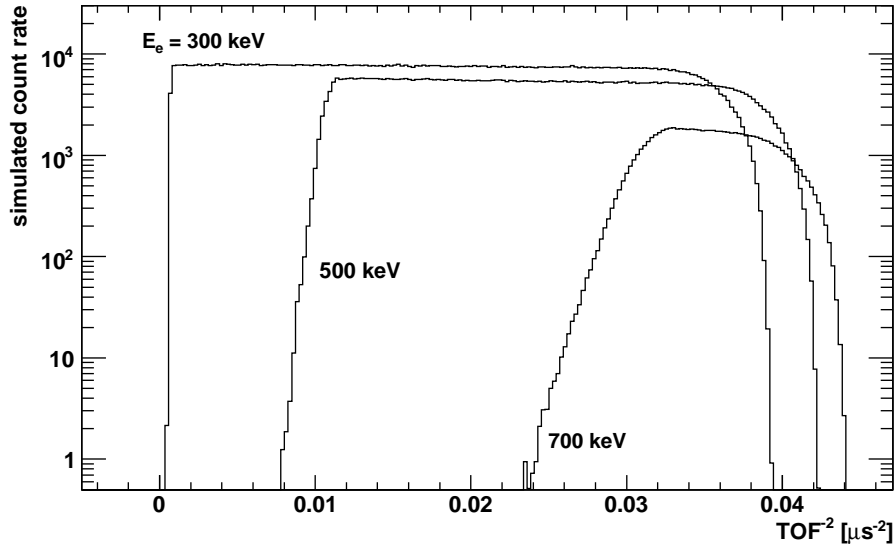


Fig. 6. Proton TOF spectra, $P_t(1=t_p^2)$, for electron kinetic energies $E_e = 300, 500$ and 700 keV, generated in a realistic GEANT4 Monte-Carlo simulation using the B field from Fig. 3 and a centered neutron beam with a width of 2 cm.

Strictly speaking, determining b requires detecting only the electron and reliably measuring its kinetic energy. Nevertheless, there are a number of challenges associated with this measurement, commented on in the following Section.

3 Measurement Uncertainties and Systematics

The statistical sensitivity of our measurement method is primarily determined by the spectrometer acceptance and imposed energy and TOF restrictions. The statistical uncertainties for our measurements of the a and b parameters in neutron decay are listed in Tab. 1, reflecting the dependence on $E_{e,m in}$, the electron kinetic energy detection threshold, and $t_{p,m ax}$, the maximum proton TOF accepted. Additionally, the electron energy calibration E_{cal} and the precise length l of the low-field drift region represent important sources of systematic uncertainty. Thus, parallel analyses will be performed keeping E_{cal} and l free, in order to study and remove their systematic effects. Table 1 shows that the reduction in statistical sensitivities under these conditions is modest.

The calculated FNPB neutron decay rate under SNS full-power conditions of $19.5/(\text{cm}^3\text{s})$, and with the Nab ductial decay volume of 20 cm^3 , yields 400 detected decays/sec [13]. In a typical 10-day run of 7×10^5 s of net beam time we would achieve $a \approx 2 \times 10^3$ and $b \approx 6 \times 10^4$. Since we plan to collect several samples of 10^9 events in several 6-week runs, the overall Nab accuracy will not be statistics-limited.

Controlling the measurement systematics presents by far the greatest challenge in the Nab experiment. The most basic task is to specify the spectrometer fields with precision sufficient for an accurate determination of the spectrometer response function $(1=t_p^2;p_p^2)$. We have adopted two methods of addressing this problem. In the first approach (Method A), we determine the shape of the spectrometer response function from theory, leaving several parameters free, to be determined by fits to the measured spectra. The second approach (Method B) relies on obtaining the detection function with its uncertainties

Table 1

Top: statistical uncertainties σ_a for the e^- correlation parameter a . A perfect spectrometer would obtain $\sigma_a = 2.3 = \frac{1}{\sqrt{N}}$. Bottom: statistical uncertainties σ_b for the Fierz interference term b .

$E_{e,m in}$	0	100 keV	100 keV	300 keV
$t_{p,m ax}$	{	{	10 s	10 s
σ_a	$2.4 = \frac{1}{\sqrt{N}}$	$2.5 = \frac{1}{\sqrt{N}}$	$2.6 = \frac{1}{\sqrt{N}}$	$3.5 = \frac{1}{\sqrt{N}}$
σ_a^y	$2.5 = \frac{1}{\sqrt{N}}$	$2.6 = \frac{1}{\sqrt{N}}$	{	{
$E_{e,m in}$	0	100 keV	200 keV	300 keV
σ_b	$7.5 = \frac{1}{\sqrt{N}}$	$10.1 = \frac{1}{\sqrt{N}}$	$15.6 = \frac{1}{\sqrt{N}}$	$26.4 = \frac{1}{\sqrt{N}}$
σ_b^{yy}	$9.1 = \frac{1}{\sqrt{N}}$	$12.7 = \frac{1}{\sqrt{N}}$	$20.3 = \frac{1}{\sqrt{N}}$	$35.1 = \frac{1}{\sqrt{N}}$

^y with E_{cal} and l variable. ^{yy} with E_{cal} and a variable.

a priori from a full description of the neutron beam and electromagnetic field geometry. Subsequently, the experimental data are fitted with only the physics observables as free parameters. Below we summarize some of the main challenges along with strategies for their control at the required level. A much more detailed discussion of both methods and the experimental challenges is given in the Nab experiment proposal [14].

Uncertainties in a due to the spectrometer response

Precise specification of the neutron beam profile: A mere 100 μ m shift of the beam center induces $\Delta a/a \approx 0.2\%$. However, this effect cancels when averaging over the two detectors on opposite sides of the solenoid; measuring a nonzero up-down proton counting asymmetry pins it down sufficiently.

Magnetic field map: The field expansion ratio defined as $r = B_{TOF} - B_0$ must be controlled at the level of $r_B = r_B = 10^{-3}$ in order to keep $\Delta a/a$ under 10^{-3} . This will be mapped out using a calibrated Hall probe. Field curvature must be determined with an accuracy of $1 \cdot 10^{-3}$ in dedicated measurements. Average mapping accuracy $\Delta B/B$ must be kept below $2 \cdot 10^{-3}$.

Flight path length: An uncertainty of order ± 30 μ m results in $\Delta a/a$ at our limit. Hence, l will be kept as a fitting parameter. Additionally, we will perform a consistency check by making differential measurement using segmented electrodes.

Homogeneity of the electric field: Electric potential will have satisfy stringent limits on inhomogeneities as discussed in the Nab proposal [14].

Rest gas: requires vacuum of 10^{-7} Pa or better.

Adiabaticity of the magnetic field configuration is not an absolute requirement. Detailed Monte Carlo analysis has shown excellent efficiency of proton momentum longitudinalization for certain relatively non-adiabatic fields. However, an adiabatic design makes the evaluation of systematic errors simpler and more reliable.

Doppler effect: Diverse effects of the Doppler effect will apparently be controlled sufficiently by the spectrometer design, but a thorough analysis will be made in conjunction with the final design.

Uncertainties in a due to the detector

Detector alignment: The spectrometer imaging properties provide for a self-consistent calibration in the data.

Electron energy calibration is required at the 10^{-4} level. To achieve it we'll use radioactive sources, evaluate directional count rate asymmetries, and also leave it as a fitting parameter with acceptably small loss of statistical sensitivity (see Tab. 1).

Trigger hermeticity is affected by the particle impact angle on the detector, backscattering, and TOF cutoff (planned in order to reduce accidental backgrounds). Several consistency checks will be evaluated from the data to

quantify and characterize the various aspects of trigger hermeticity.

TOF measurement uncertainties: The requirement is $(\frac{\delta}{t_e} \approx \frac{\delta t_e}{t_e}) \approx 100$ ps. While it is not necessary to reach this timing accuracy for each event, it has to be achieved for the event sample average, a realistic goal given the planned event statistics.

Edge effects introduce important systematicatics. Thanks to the imaging properties of the spectrometers, these can be controlled and corrected for to a sufficient degree with appropriate cuts on the data.

Uncertainties in b

Sources of uncertainties in the measurement of b are fewer than for a since accurate proton momentum measurement (via its TOF) is not required. The dominant sources are electron energy calibration (discussed above) and electron backgrounds.

Backgrounds for a and b

Neutron beam related backgrounds are notoriously hard to calculate and model a priori, and will ultimately have to be measured and characterized in situ. Reasonable estimates place the beam-related background rates below the signal rate. While we have plans for shielding and lining surfaces with neutron absorbing ^6LiF material, the coincident technique of detecting e^+e^- pairs helps to reduce substantially the effect of beam-related accidental backgrounds.

Particle trapping: Electrons can be trapped in the decay volume, expansion, and TOF regions. These regions form an electrode-less Penning trap. The potential well trap does not cause a problem for electrons above our energy threshold. The longitudinalization of the electron momentum due to the magnetic field allows all of them to escape and to reach the detector. Low energy electrons from neutron decay, from field ionization or from rest gas interactions are a concern since trapped particles ionize the rest gas, and the ions form a time-dependent background. Several strategies are under consideration to remove the trapped particles; they will be refined under real running conditions.

4 Summary

The Nab collaboration plans simultaneous high-statistics measurements of neutron decay parameters a , the e^+e^- correlation coefficient, and b , the Fierz interference term, with $a \approx 10^{-3}$ and $b \approx 3 \cdot 10^{-3}$.

Basic properties of the Nab spectrometer are well understood; details of the fields are under study in extensive analytical and Monte Carlo calculations.

Elements of the proposed Nab spectrometer will be shared with other neutron decay experiments, such as abBA.

Development of the abBA/Nab Si detectors is ongoing and remains a technological challenge. Each of the target properties of the detector have been realized separately; the remaining task is to realize them simultaneously in one piece of silicon.

The major elements of the data acquisition system have been successfully developed.

The experiment received approval in Feb. 2008. Under the most favorable funding and technical scenario it could be ready for commissioning in 2010.

References

- [1] A. Czamecki, W. J. Marciano, and A. Sirlin, *Phys. Rev. D* 70 (2004) 093006.
- [2] P. Herczeg, *Prog. Part. Nucl. Phys.* 46 (2001) 413.
- [3] N. Severijns, M. Beck, O. Naviliat-Cuncic, *Rev. Mod. Phys.* 78 (2006) 991.
- [4] M. J. Ramsey-Musolf and S. Su, *Phys. Rept.* 456 (2008) 1.
- [5] J. D. Jackson, *Phys. Rev.* 106 (1957) 517.
- [6] V. Gudkov, G. L. Greene and J. R. Calarco, *Phys. Rev. C* 73 (2006) 035501.
- [7] W. Yao, et al., *J. Phys. G* 33, 1 (2006).
- [8] Nab experiment homepage: <http://nab.phys.virginia.edu>.
- [9] S. Baessler et al., to appear soon in *Eur. Phys. J.* (2008).
- [10] F. E. Wietfeldt, et al., *Nucl. Instr. and Meth. Phys. Res. A* 545 (2005) 181.
- [11] J. D. Bowman, *J. Res. NIST* 110 (2005) 407.
- [12] <http://geant4.web.cern.ch/geant4/>.
- [13] P. R. Human, et al., "Beam line Performance Simulations for the FnPB", private communication, 2005. Initial measurements performed in the FnPB up to the time of this writing are in agreement with the simulation.
- [14] http://nab.phys.virginia.edu/nab_proposal.pdf.